Inorg. Chem. **2004**, *43*, 8437–8446

Electrochemical Generation of Free Nitric Oxide from Nitrite Catalyzed by Iron *meso*-Tetrakis(4-*N*-methylpyridiniumyl)porphyrin

Yuwu Chi,* Jingyuan Chen, and Koichi Aoki

Department of Applied Physics, Faculty of Engineering, University of Fukui, 3-9-1 Bunkyo, Fukui-shi 910-8507, Japan

Received May 25, 2004

Electrochemical generation of free nitric oxide (NO) from nitrite (NO_2^-) catalyzed by iron *meso*-tetrakis(4-*N*-methylpyridiniumyl)porphyrin, $[Fe^{III}(TMPyP)]^{5+}$, has been developed in this study. To obtain free NO, a cathodic electrolysis and an anodic electrolysis were performed in two connected flow electrolytic cells in sequence. The flow electrolytic cell upstream was used for cathodic electrolysis, where the solution of $[Fe^{III}(TMPyP)]^{5+}$ and NO_2^- was reduced at –0.25 V (vs Ag/AgCl) into $[Fe^{II}(NO_2^-)_2(TMPyP)]^{2+}$ and $[Fe^{II}(NO)(TMPyP)]^{4+}$ in sequence. The flow electrolytic cell downstream was utilized for anodic electrolysis, where $[Fe^{II}(NO)(TMPyP)]^{4+}$ formed from the upstream cell was oxidized at +0.40 V (vs Ag/AgCl) into $[Fe^{III}(TMPyP)]^{5+}$ and free NO. Finally, NO was bubbled out from anodic electrolyte by argon gas. The mechanism and the optimum conditions for electrochemical generation of NO from NO_2^- catalyzed by $[Fe^{III}(TMPyP)]^{5+}$ were studied in detail by voltammetric and spectroelectrochemical methods.

Introduction

NO has been recognized recently as one of the most important physiological regulators.[1] It plays an important role as a biological second messenger in different functions of the human body, for vascular smooth muscle relaxation for blood pressure lowering and inhibition of platelet aggregation[2−5] and for cellular communication,[6] and even acts as a major defense molecule in the immune system, for killing bacteria and tumor cells.[7] In the body, NO can be produced by heme-containing nitric oxide synthetase from L-arginine in the endothelial as well as other cells upon interaction with inducing agents such as acetylcholine, bradykinin, adenine nucleotides, thrombin, and serotonin,[8,9] or NO can be generated from the decomposition of vasodilator drugs such as nitroglycerin.[10]

However, it is difficult to control the release of NO and its distribution in the body by using either inducing agents or vasodilator drugs. Thus, a controllable method for generation of NO in a local target part of the body is of great clinical interest in terms of improving efficiency of therapy and avoiding undesirable side effects, for example, release of NO locally to prevent the formation of thrombus without causing a decrease of blood pressure, or generation of NO in tumor tissue to kill tumor cells without killing normal cells of the body. Recently, polymeric films capable of continuously releasing low levels of NO have been studied for improving the thromboresistivity and antibacterial ability of biomedical devices.[11−22] However, application of these NO release polymeric films is limited by their short lifetime

* Author to whom correspondence should be addressed. E-mail: y.w.chi@asura.apphy.fukui-u.ac.jp. Phone: (81)-90-82676873.

(1) Koshland, D. E., Jr. *Science* **1992**, *258*, 1861.
(2) Furchgott, R. F.; Zawadski, J. V. *Nature* **1980**, *288*, 373−376.
(3) Ignarro, L. I.; Buga, C. M.; Wood, K. S.; Byrns, R. E. *Proc. Natl. Acad. Sci. U.S.A.* **1987**, *84*, 9265−9269.
(4) Palmer, R. M. J.; Ferrige, A. G.; Moncada, S. *Nature* **1987**, *327*, 524−526.
(5) Synder, S. H. *Science* **1992**, *257*, 494−496.
(6) Knowles, R. G.; Palacios, M.; Palmer, R. M. J.; Moncada, S. *Proc. Natl. Acad. Sci. U.S.A.* **1989**, *86*, 5159−5162.
(7) Hibbs, J. B.; Taintor, R. R.; Vavrin, Z.; Rachlin, E. M. *Biochem. Biophys. Res. Commun.* **1988**, *157*, 87−94.
(8) Palmer, R. M. J.; Ashton, D. S.; Moncada, S. *Nature* **1988**, *333*, 664−666.
(9) Moncada, S.; Palmer, R. M. J.; Higgs, E. A. *Hypertension* **1988**, *12*, 365−372.
(10) Katsuki, S.; Arnold, W.; Mittal, C.; Murad, F. J. *Cyclic Nucleotide Res.* **1977**, *3* (1), 23−35.
(11) Smith, D. J.; Chakravarthy, D.; Pulfer, S.; Simmons, M. L.; Hrabie, J. A.; Citro, M. L.; Saavedra, J. E.; Davies, K. M.; Hustsell, T. C.; Mooradian, D. L.; Hanson, S. R.; Keefer, L. K. *J. Med. Chem.* **1996**, *39*, 1148−1156.
(12) Mowery, K. A.; Schoenfisch, M. H.; Baliga, N.; Wahr, J. A.; Meyerhoff, M. E. *Electroanalysis* **1999**, *11*, 681−686.
(13) Ramamurthi, A.; Lewis, R. S. *Ann. Biomed. Eng.* **2000**, *28*, 174−181.
(14) Bohl, K. S.; West, J. L. *Biomaterials* **2000**, *21*, 2273−2278.
(15) Mowery, K. A.; Schoenfisch, M. H.; Savedra, J. E.; Keefer, L. K.; Meyerhoff, M. E. *Biomaterials* **2000**, *21*, 9−21.

10.1021/ic049323c CCC: $27.50
Published on Web 12/02/2004

because only a small amount of NO adducts can be loaded within thin coatings of the polymeric materials. It has been revealed that nitrite (NO_2^-), a common metabolic product in the biological system, can be reduced to NO by iron porphyrin-containing nitrite reductase[23] and various model enzymes (usually iron porphyrins).[24−32] Further studies in this field showed that NO could also be produced as an intermediate or a main product during the electrochemical reduction of NO_2^- in the presence of iron porphyrins.[33−39] Apparently, these studies imply that, upon catalysis of iron porphyrins, a low level of NO can be electrochemically generated in the body from NO_2^-, the concentration of which ranges from 0.5 to 10 μM in plasma, erythrocytes, and tissues,[40] and thus, an electrochemically controllable method for a low level of NO release at a local site in the body can be developed. However, to control the electrochemical generation of NO, there are still several problems to solve, among which the conversion rate of nitrite to NO is most important. A high yield of coordinated NO was obtained when using water-insoluble octaethylporphrin iron(III) chloride, Fe(OEP)Cl;[39] however, the reaction can only be carried out in nonaqueous media, which is unfit for generating NO under the physiological condition. On the contrary, when using water-soluble iron porphyrins, such as $[Fe^{III}(TPPS)]^{3-}$[34] and $[Fe^{III}(TMPyP)]^{5+}$,[35] the yield of NO was very low, which mainly resulted from further reduction of coordinated NO to ammonia and other species under high negative potential (<-0.65 V vs SCE) conditions employed in these studies. Therefore, to improve the yield of NO by using these water-soluble iron porphyrins, the potential condition as well as reaction kinetics should be studied in detail. Another problem to be solved is how to obtain free NO. During the reduction of NO_2^- based on the catalysis of iron porphyrin, NO is usually produced in coordinated form, i.e., complexes of NO with iron porphyrin, the stability of which varies with the type of ligands and the valence of the central metal.[41] So this problem should also be considered and solved to obtain free NO.

In this study, we examined the electrocatalysis of the water-soluble porphyrin $[Fe^{III}(TMPyP)]^{5+}$ for the reduction of nitrite to nitric oxide under the physiological pH condition (pH7.4) and, on this basis, developed an electrochemical generation method for free NO.

Experimental Section

Chemicals. 5,10,15,20-Tetrakis(*N*-methylpyridinium-4-yl)-21*H*,23*H*-porphine, tetrakis(*p*-toluenesulfonate), or $[H_2(TMPyP)]\cdot 4Ts$, obtained from Dojindo (Japan) was used for preparation of $[Fe^{II}(TMPyP)]Cl_4$ and $[Fe^{III}(TMPyP)]Cl_5$ without further purification. Sodium nitrite (from Wako, Japan) and other chemicals used were of analytical reagent purity. All solutions were prepared by using twice-distilled water.

Preparation of $[Fe^{II}(TMPyP)]Cl_4$ was carried out in the following way: 100 mL of 1.0×10^{-3} mol·L $^{-1}$ $[H_2(TMPyP)]Cl_4$ solution produced by ion exchange of 0.1364 g of $[H_2(TMPyP)]\cdot 4Ts$ was heated at reflux and simultaneously degassed by ultrapure argon gas to remove oxygen from the system completely. Five hours later, the solution was added with equivalent moles of $FeCl_2\cdot 4H_2O$ (0.0199 g) and continuously heated at reflux for 15 h, during which 2 equiv of NaOH (8 mg) was added to neutralize HCl formed during the reaction. Finally, 100 mL of 1.0×10^{-3} mol·L $^{-1}$ $[Fe^{II}(TMPyP)]Cl_4$ solution was obtained and cooled to room temperature, with a yield of higher than 95%. $[Fe^{II}(TMPyP)]Cl_4$ synthesized by this method showed electronic absorption spectral data of λ_{max} (log ϵ) = 445 (5.05), 560 (3.98), and 610 (3.63), in pH 7.4 PBS, which were consistent with those of $[Fe^{II}(TMPyP)]Cl_4$ chemically reduced from $[Fe^{III}(TMPyP)]Cl_5$ by ascorbate.[42] Since NaCl formed from the neutralization of HCl by NaOH did not interfere with the spectral and electrochemical measurements, the synthesized $[Fe^{II}(TMPyP)]Cl_4$ solution was then used without further purification. Because $[Fe^{II}(TMPyP)]Cl_4$ was found to be very readily oxidized by oxygen when exposed to the air, it was protected rigidly by high-purity argon during the whole process of its synthesis, storage, and measurement.

$[Fe^{III}(TMPyP)]Cl_5$ solution was obtained after oxygen gas was bubbled into $[Fe^{II}(TMPyP)]Cl_4$ solution for 12 h. It showed electronic absorption spectral data of λ_{max} (log ϵ) = 424 (4.98), 605 (3.75), and 640 (3.58), in pH 7.4 PBS, which were consistent with those of $[Fe^{III}(TMPyP)]Cl_5$ prepared by the Pasternack method.[43]

(16) Schoenfisch, M. H.; Mowery, K. A.; Rader, M. V.; Baliga, N.; Wahr, J. A.; Meyerhoff, M. E. *Anal. Chem.* **2000**, *72*, 1119−1126.
(17) Robbins, M. E.; Chen, T. Y.; Schoenfishch, M. H. *J. Am. Chem. Soc.* **2001**, *123*, 9712−9713.
(18) Zhang, H.; Annich, G. M.; Miskulin, J.; Osterholzer, K.; Merz. S. I.; Bartlett, R. H.; Meyerhoff, M. E. *Biomaterials* **2002**, *23*, 1485−1494.
(19) Frost, M. C.; Rudich, S. M.; Zhang, H.; Maraschio, M. A.; Meyerhoff, M. E. *Anal. Chem.* **2002**, *74*, 5942−5947.
(20) Marxer, S. M.; Rothrock, A. R.; Nablo, B. J.; Robbins, M. E.; Schoenfisch, M. H. *Chem. Mater.* **2003**, *15*, 4193−4199.
(21) Robbins, M. E.; Schoenfishch, M. H. *J. Am. Chem. Soc.* **2003**, *125*, 6068−6069.
(22) Frost, M. C.; Meyerhoff, M. E. *J. Am. Chem. Soc.* **2004**, *126*, 1348−1349.
(23) Silvestrini, M. C.; Falcinelli, S.; Ciabatti, I.; Cutruzzola, F.; Brunori, M. *Biochimie* **1994**, *76*, 641−654.
(24) Shimada, H.; Orii, Y. *FEBS Lett.* **1975**, *54*, 237−240.
(25) Stolzenberg, A. M.; Strauss, S. H.; Holm, R. H. *J. Am. Chem. Soc.* **1981**, *103*, 4763−4778.
(26) Fujita, E.; Fajer, J. *J. Am. Chem. Soc.* **1983**, *105*, 6743−6745.
(27) Kim, C. H.; Hollocher, T. C. *J. Biol. Chem.* **1984**, *259*, 2092−2099.
(28) Finnegan, M. G.; Lappin, A. G.; Scheidt, W. R. *Inorg. Chem.* **1990**, *29*, 181−185.
(29) Silvestrini, M. C.; Tordi, M. G.; Musci, G.; Brunori, M. *J. Biol. Chem.* **1990**, *265*, 11783−11787.
(30) Ye, R. W.; Toro-suarez, I.; Tiedje, J. M.; Averill, B. A. *J. Biol. Chem.* **1991**, *266*, 12848−12851.
(31) Ozawa, S.; Fujii, H.; Morishima, I. *J. Am. Chem. Soc.* **1992**, *114*, 1548−1554.
(32) Ozawa, S.; Sakamoto, E.; Ichikawa, T.; Watanabe, Y.; Morishima, I. *Inorg. Chem.* **1995**, *34*, 6363−6370
(33) Fernandes, J. B.; Feng, D.; Chang, A.; Keyser, A.; Ryan, M. D. *Inorg. Chem.* **1986**, *25*, 2606−2610.
(34) Barley, M. H.; Takeuchi, K. J.; Meyer, T. J. *J. Am. Chem. Soc.* **1986**, *108*, 5876−5885.
(35) Barley, M. H.; Rhodes, M. R.; Meyer, T. J. *Inorg. Chem.* **1987**, *26*, 1746−1750. Younathan, J. N.; Wood, K. S.; Meyer, T. J. *Inorg. Chem.* **1992**, *31*, 3280−3285.
(36) Cheng, S. H.; Su Y. O. *Inorg. Chem.* **1994**, *33*, 5847−5854.
(37) Bedioui, F.; Trevin, S., Albin, V.; Villegas, M. G. G.; Devynck, J. *Anal. Chim. Acta* **1997**, *341*, 177−185.
(38) Chen, J. Y.; Ikeda, O. *Electroanalysis* **2001**, *13* (13), 1076−1081.
(39) Wei, Z. C.; Ryan, M. D. *Inorg. Chim. Acta* **2001**, *314*, 49−57.
(40) Rodriguez, J.; Maloney, R. E.; Rassaf, T.; Bryan, N. S.; Feelisch, M. *Proc. Natl. Acad. Sci. U.S.A.* **2003**, *100*, 336−341.
(41) Hoshino, M.; Ozawa, K.; Seki, H.; Ford, P. C. *J. Am. Chem. Soc.* **1993**, *115*, 9568−9575.
(42) Tondreau, G. A.; Wilkins, R. G. *Inorg. Chem.* **1986**, *25*, 2745−2750.
(43) Pasternack, R. F.; Lee, H.; Malek, P.; Spencer, C. J. *Inorg. Nucl. Chem.* **1977**, *39*, 1865.

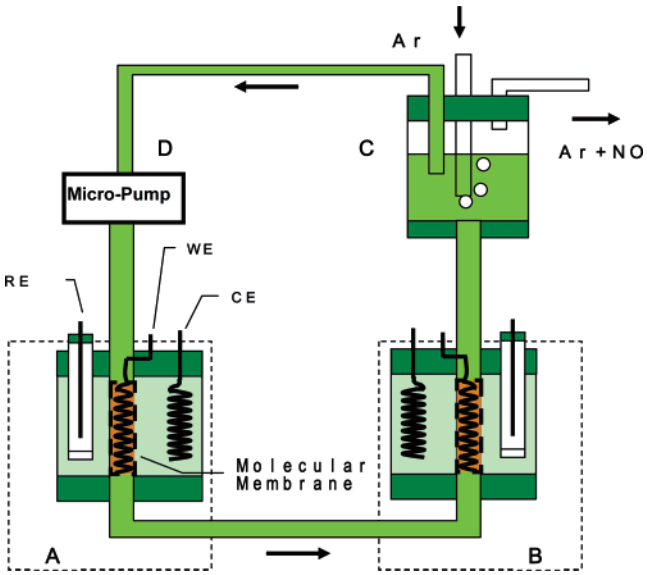

Figure 1. Schematic diagram of the system for electrochemical generation of NO: (A, B) flow electrolytic cells; (C) solution reservoir; (D) micropump.

Solutions saturated with NO were prepared by bubbling 1% NO gas (Nippon Sanso, Japan) into deoxygenated solutions for 30 min, and their concentrations were evaluated from Ostwald's solubility coefficient for a given partial pressure of NO.[44] All solutions were deoxygenated by ultrapure argon gas for 15 min before electrochemical and spectral measurements, and protected by an argon atmosphere during the measurements.

Unless mentioned otherwise, the aqueous medium used was a 0.1 mol·L^{-1}, pH 7.4 sodium phosphate buffer solution (PBS).

Apparatus. A potentiostat (Huso electrochemical system, model 1112, Japan) combined with a three-electrode system was used for all electrochemical experiments. A Pt disk working electrode (0.071 cm^2 area) was used for voltammetric measurements; a Pt mesh (The Nilaco Co., Japan) working electrode with 50% transmittance was placed in a spectrophotometric cell (0.4 mm light path length) and used for spectroelectrochemical measurements. The other two electrodes for the three-electrode system were a Ag/AgCl reference electrode and a Pt coil auxiliary electrode.

A Cray50 (Varian Australia Pty Ltd.) spectrophotometer was used for measurements of electronic absorption spectra.

A system (see Figure 1) consisting of two flow electrolytic cells (A, B), a micropump (D), and a solution reservoir (C) was used for electrochemical generation of NO from NO_2^- based on the catalysis of $[Fe^{III}(TMPyP)]^{5+}$. The structure of the flow electrolytic cell was similar to that used by Fujinaga et al.[45] except that the working electrode used in our study was Pt coils and was separated from the other two electrodes (reference electrode and auxiliary electrode) by a molecular porous membrane (Spectrum Laboratories Inc.) with an MWCO of 1000. The micropump was a Masterflex C/L pump system (Cole-Parmer Instrument Co.), which could control the flow rate of solution from several microliters per minute to several milliliters per minute. The solution reservoir was used to contain $[Fe^{III}(TMPyP)]^{5+}$ and $NaNO_2$ and bubbled with argon gas to transfer NO (electrochemically produced) from the solution phase to the gas phase. A NO gas sensor (Gastec Co., Japan) was used to detect the concentration of NO in the gas phase in the solution reservoir.

(44) Lide, D. R. *CRC Handbook of Chemistry Physics*, 76th ed.; CRC Press: Boca Raton, FL, 1995; Section 6-3.
(45) Fujinaga, T.; Kihara, S. *CRC Crit. Rev. Anal. Chem.* **1977**, *6*, 223.

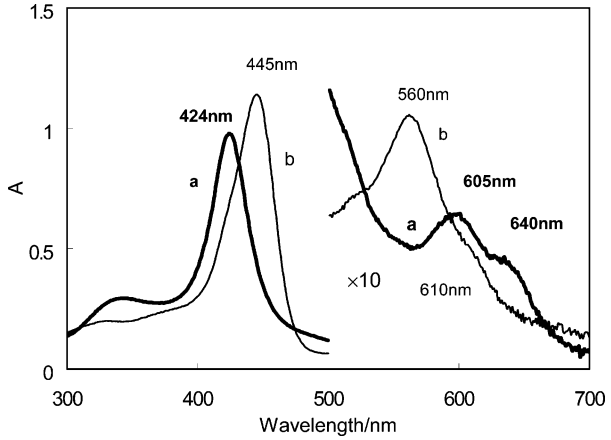

Figure 2. Electronic absorption spectra obtained for (a) 2.5×10^{-4} mol·L^{-1} $[Fe^{III}(TMPyP)]^{5+}$ and (b) 2.5×10^{-4} mol·L^{-1} $[Fe^{II}(TMPyP)]^{4+}$ in pH 7.4 PBS buffer.

Results

Interaction of NO and NO_2^- with $[Fe^{III}(TMPyP)]^{5+}$ and $[Fe^{II}(TMPyP)]^{4+}$. The electronic absorption spectra of $[Fe^{III}(TMPyP)]^{5+}$ and $[Fe^{II}(TMPyP)]^{4+}$ at pH 7.4 are shown in Figure 2. $[Fe^{III}(TMPyP)]^{5+}$ exhibits a strong Soret band at 424 nm and weak Q-bands at 605 and 640 nm (curve a in Figure 2), whereas $[Fe^{II}(TMPyP)]^{4+}$ has a Soret band at 445 nm and Q-bands at 560 and 610 nm (curve b in Figure 2). It was found that the absorption spectrum of $[Fe^{III}(TMPyP)]^{5+}$ did not change in the presence of NO or NO_2^-, indicating that neither NO_2^- nor NO complexes with $[Fe^{III}(TMPyP)]^{5+}$. Recently, Trofimova and co-workers reported that a high concentration of NO (>5%) could react with $[Fe^{III}(TMPyP)]^{5+}$ via the reaction[46]

$$[Fe^{III}(TMPyP)]^{5+} + 2NO + H_2O \rightarrow [Fe^{II}(NO)(TMPyP)]^{4+} + NO_2^- + 2H^+ \quad (1)$$

Apparently, this equation includes a redox reaction rather than a complex reaction between $[Fe^{III}(TMPyP)]^{5+}$ and NO, which indicates that $[Fe^{III}(TMPyP)]^{5+}$ cannot complex with NO to produce such a complex as $[Fe^{III}(NO)(TMPyP)]^{5+}$. In contrast, both NO and NO_2^- complexed with $[Fe^{II}(TMPyP)]^{4+}$, which was confirmed by the obvious change of the spectra. Figure 3 shows that, when NO was bubbled into $[Fe^{II}(TMPyP)]^{4+}$ solution, the band at 610 nm disappeared, the band at 560 nm shifted to 550 nm, and the Soret band at 445 nm shifted to 426 nm. The final spectrum was the same as that of $[Fe^{II}(NO)(TMPyP)]^{4+}$,[38,46] so this complex reaction can be proposed as the following:

$$[Fe^{II}(TMPyP)]^{4+} + NO \rightarrow [Fe^{II}(NO)(TMPyP)]^{4+} \quad (2)$$

In the case of the complex reaction between $[Fe^{II}(TMPyP)]^{4+}$ and NO_2^- (see Figure 4), with the decrease of the band at 560 nm, a new band was first observed to appear quickly at 540 nm (curve b in Figure 4); this new absorption band has been suggested to come from the Q-band of $[Fe^{II}(NO_2^-)(TMPyP)]^{3+}$ formed in the solution.[38] However,

(46) Trofimova, N. S.; Safronov, A. Y.; Ikeda, O. *Inorg. Chem.* **2003**, *42*, 1945−1951.

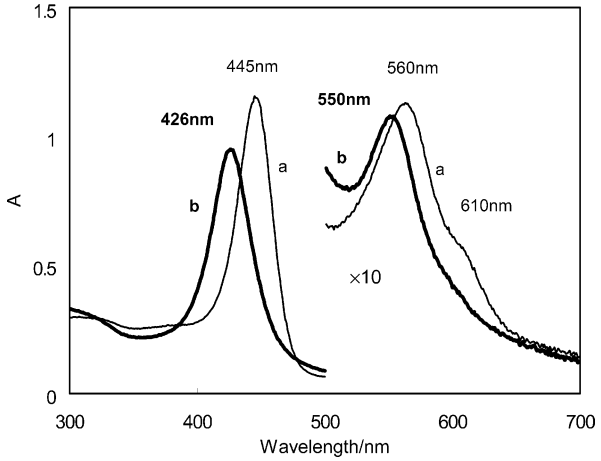

Figure 3. Electronic absorption spectral changes obtained for a 2.5×10^{-4} mol·L^{-1} $[Fe^{II}(TMPyP)]^{4+}$ solution: (a) before and (b) after being bubbled with 1% NO gas.

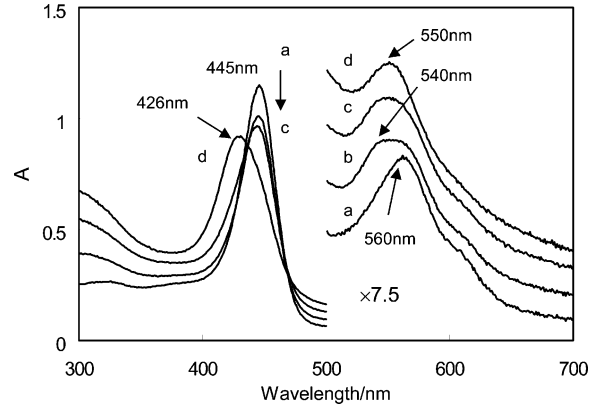

Figure 4. Electronic absorption spectral changes obtained for the solution containing 2.5×10^{-4} mol·L^{-1} $[Fe^{II}(TMPyP)]^{4+}$ and 2.5×10^{-2} mol·L^{-1} $NaNO_2$. The spectra were recorded at times (a) 0, (b) 1, (c) 5, and (d) 20 min after the solution was prepared.

our experimental results (described below) showed that in the presence of a high concentration of NO_2^-, $[Fe^{II}(NO_2^-)_2(TMPyP)]^{2+}$ rather than $[Fe^{II}(NO_2^-)(TMPyP)]^{3+}$ was formed. Five minutes after the reaction began (see curves c and d in Figure 4), the band at 540 nm shifted slowly to 550 nm (assigned to $[Fe^{II}(NO)(TMPyP)]^{4+}$ by curve b in Figure 3), which means that $[Fe^{II}(NO_2^-)_2(TMPyP)]^{2+}$ is unstable and can spontaneously change to $[Fe^{II}(NO)(TMPyP)]^{4+}$. This result supports the viewpoint that the instability of iron porphyrin−nitrite complexes results from the extreme thermodynamic stability of the iorn(II)−nitrosyl.[47]

Electrochemical Generation of $[Fe^{II}(NO_2^-)_2(TMPyP)]^{2+}$. Cyclic voltammetric measurements were carried out for $[Fe^{III}(TMPyP)]^{5+}$ in the presence of various concentrations of $NaNO_2$. Figure 5a shows that, in the absence of NO_2^- at pH 7.4, $[Fe^{III}(TMPyP)]^{5+}$ exhibits a couple of well-defined redox peaks at −0.110 and −0.175 V, which has been confirmed to involve a reversible one-electron-transfer process:[35]

$$[Fe^{III}(TMPyP)]^{5+} + e^- \leftrightarrow [Fe^{II}(TMPyP)]^{4+} \qquad (3)$$

However, in the presence of NO_2^- (Figure 5b,c) the redox

(47) Wyllie, G. R. A.; Scheidt, W. R. *Chem. Rev.* **2002**, *102*, 1067−1089.

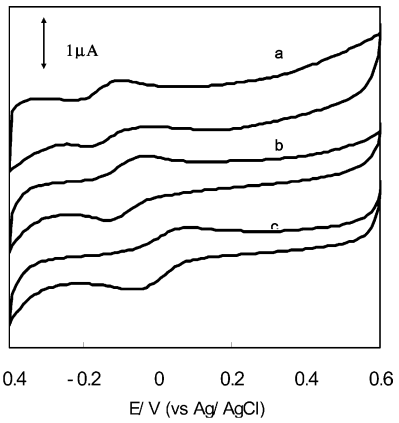

Figure 5. Cyclic voltammograms obtained for 2.5×10^{-4} mol·L^{-1} $[Fe^{III}(TMPyP)]^{5+}$ at the Pt electrode in the presence of $NaNO_2$ of various concentrations: (a) 0, (b) 2.5×10^{-3}, (c) 2.5×10^{-2} mol·L^{-1}. The scan rate was 10 mV·s^{-1}.

peaks shift to more positive potentials with increasing concentration of NO_2^-. This appears to result from the formation of a nitrite−ferrous porphyrin complex in the solution. The coordination number of NO_2^- in the nitrite−ferrous porphyrin complex can be obtained by using Nernst equation:

$$E_{1/2} = E_K + 0.059 \log [NO_2^-]^n = E_K + 0.059n \log [NO_2^-] \qquad (4a)$$

where $E_{1/2}$ is the half-wave potential of ferric/ferrous oxidation, E_K is a constant, and n is the coordination number of NO_2^- in the iron(II)−nitrite complex. When the mole ratio of nitrite to iron porphyrin ($C_{NO_2^-}/C_{FeP}$) is high enough (>10), i.e., $[NO_2^-] \approx C_{NO_2^-}$, we can obtain the following equation:

$$E_{1/2} \approx E_K + 0.059n \log cNO_2^- = (E_K + 0.059n \log c_{FeP}) + 0.059n \log\left(\frac{c_{NO_2^-}}{c_{FeP}}\right)$$

$$= E_{K'} + 0.059n \log\left(\frac{c_{NO_2^-}}{c_{FeP}}\right) \qquad (4b)$$

According to eq 4b, a plot of $E_{1/2}$ vs the mole ratio of log($C_{NO_2^-}/C_{FeP}$) was made and is shown in Figure 6. It was evident that there was a good linear relationship between $E_{1/2}$ and log($C_{NO_2^-}/C_{FeP}$) at a high mole ratio of nitrite to porphyrin (>10). A slope of 110 mV was obtained, indicating that the coordination number, n, was 2, i.e., bisnitrite−ferrous porphyrin was produced (reaction 5).

$$[Fe^{III}(TMPyP)]^{5+} + e^- + 2NO_2^- \leftrightarrow [Fe^{II}(NO_2^-)_2(TMPyP)]^{2+} \qquad (5)$$

In this study, because $[Fe^{III}(TMPyP)]^{5+}$ was used as a catalyst, its concentration was about 100 times less than that of NO_2^-, i.e., nitrite concentration ≫ 10 equiv of porphyrin; it was evident that $[Fe^{II}(NO_2^-)_2(TMPyP)]^{2+}$ was dominant during the reactions. According to the cyclic voltammogram shown in Figure 5, a suitable potential for electrochemical generation of $[Fe^{II}(NO_2^-)_2(TMPyP)]^{2+}$ was about −0.25 V

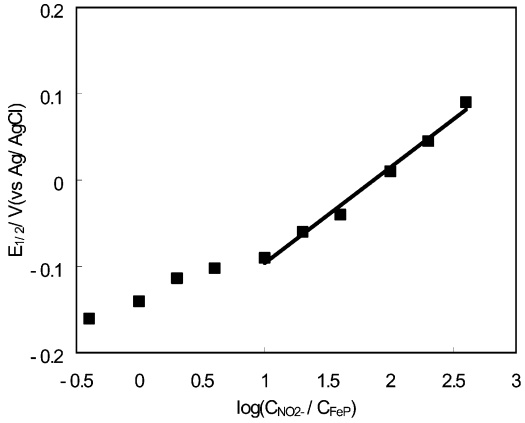

Figure 6. Variation of the oxidation half-wave potential ($E_{1/2}$) of ferrous iron porphyrin (2.5×10^{-4} mol·L^{-1}) with the mole ratio of $C_{NO^{2-}}/C_{FeP}$. The scan rate was 10 mV·s^{-1}.

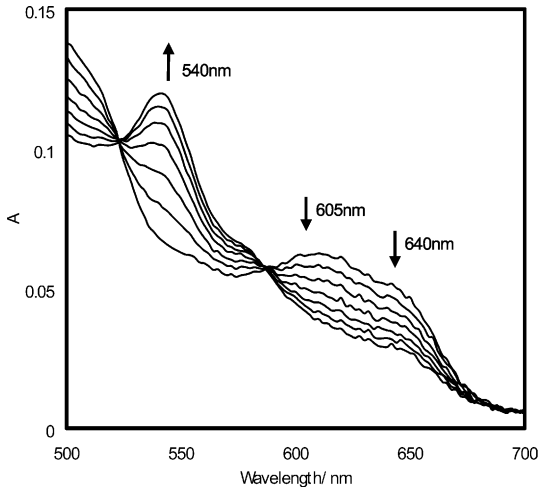

Figure 7. Electronic absorption spectral changes obtained for the solution containing 2.5×10^{-4} mol·L^{-1} $[Fe^{III}(TMPyP)]^{5+}$ and 2.5×10^{-2} mol·L^{-1} $NaNO_2$ during electrolysis at -0.25 V. The spectra were recorded within 2 min.

(vs Ag/AgCl). Then, at this potential, the electrochemical generation of $[Fe^{II}(NO_2^-)_2(TMPyP)]^{2+}$ was observed by spectroelectrochemistry. $[Fe^{II}(NO_2^-)_2(TMPyP)]^{2+}$ formed rapidly from a mixed solution of $[Fe^{III}(TMPyP)]^{5+}$ and NO_2^- when a -0.25 V potential was applied, which was confirmed by the fact that the Q-bands at 605 and 640 nm decreased while a new band at 540 nm increased gradually (see Figure 7). A reverse spectral change was observed (data not shown) upon applying a $>+0.1$ V potential, as soon as $[Fe^{II}(NO_2^-)_2(TMPyP)]^{2+}$ was produced. This confirms that the electrochemical generation of $[Fe^{II}(NO_2^-)_2(TMPyP)]^{2+}$ (shown in eq 5) is reversible.

Disproportionation of $[Fe^{II}(NO_2^-)_2(TMPyP)]^{2+}$. As described above, the study on the interaction of $[Fe^{II}(TMPyP)]^{4+}$ and NO_2^- (see Figure 4) has shown that $[Fe^{II}(NO_2^-)_2(TMPyP)]^{2+}$ can spontaneously change to its reduced form, $[Fe^{II}(NO)(TMPyP)]^{4+}$. In terms of redox equilibrium, a corresponding oxidized species such as $[Fe^{III}(TMPyP)]^{5+}$ or NO_3^- should be produced at the same time. To ensure this, the spectral change of $[Fe^{II}(NO_2^-)_2(TMPyP)]^{2+}$ with time was recorded at open circuit potential. Figure 8 shows that, upon standing, Q-band absorption at 540 nm

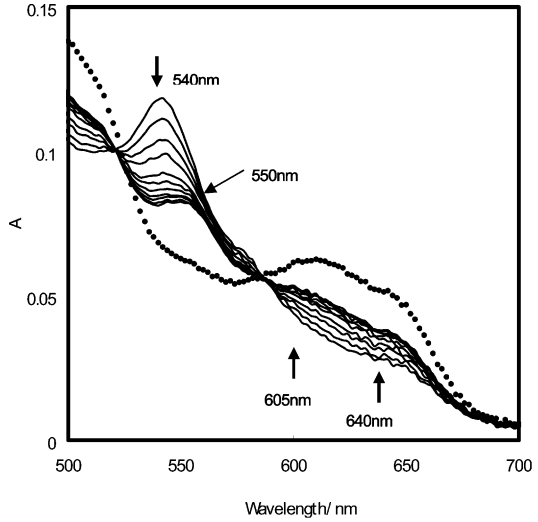

Figure 8. Electronic absorption spectral changes of $[Fe^{II}(NO_2^-)_2(TMPyP)]^{2+}$ with time at open circuit potential. The spectra (solid lines) were recorded within 6 min and compared with that of $[Fe^{III}(TMPyP)]^{5+}$ (dotted line).

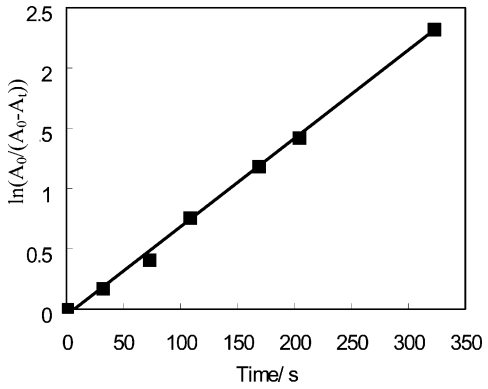

Figure 9. $\ln(A_0/(A_0 - A_t))$ versus time (s). A_0 and A_t are the absorbance at 540 nm at reaction time 0 and t, respectively. The data were obtained from Figure 8.

associated with $[Fe^{II}(NO_2^-)_2(TMPyP)]^{2+}$ decreased and shifted to 550 nm (the characteristic band of $[Fe^{II}(NO)(TMPyP)]^{4+}$), and simultaneously, new absorptions at 605 and 640 nm corresponding to $[Fe^{III}(TMPyP)]^{5+}$ appeared; thus, it is confirmed that, at pH 7.4, $[Fe^{II}(NO_2^-)_2(TMPyP)]^{2+}$ can change to $[Fe^{II}(NO)(TMPyP)]^{4+}$ and $[Fe^{III}(TMPyP)]^{5+}$ via disproportionation. Furthermore, Figure 8 also shows that half the amount of $[Fe^{II}(NO_2^-)_2(TMPyP)]^{2+}$ was reduced to $[Fe^{II}(NO)(TMPyP)]^{4+}$ whereas the other half of the amount of $[Fe^{II}(NO_2^-)_2(TMPyP)]^{2+}$ was oxidized to $[Fe^{III}(TMPyP)]^{5+}$. Thus, the disproportionation reaction can be proposed as the following:

$$2[Fe^{II}(NO_2^-)_2(TMPyP)]^{2+} + H_2O \rightarrow$$

$$[Fe^{II}(NO)(TMPyP)]^{4+} + [Fe^{III}(TMPyP)]^{5+} + 3NO_2^- + 2OH^- \quad (6a)$$

According to the change of absorptions at 540 nm ($A_0 - A_t$), we plotted $\ln(A_0/(A_0 - A_t))$ vs time in Figure 9, and found there was a good linear relationship ($R^2 = 0.9981$) between $\ln(A_0/(A_0 - A_t))$ and reaction time. Thus, the disproportionation reaction was recognized to be a first-order reaction,

with a rate constant of $(7.30 \pm 0.36) \times 10^{-3}$ s^{-1} and half-life time of 95 ± 5 s ($n = 7$, confidence level 95%), when pH 7.4 PBS buffer was used as the reaction medium. The same conclusion can be drawn when the spectral data at 605 and 640 nm are analyzed. The recognition of a first-order reaction means that reaction 6a is not a basic reaction but an overall reaction, which includes a rate-determining reaction step. This rate-determining step, i.e., the slowest step should be a first-order reaction. On this basis, we propose that the disproportionation of $[Fe^{II}(NO_2^-)_2(TMPyP)]^{2+}$ shown in reaction 6a probably undergoes the following steps:

$$[Fe^{II}(NO_2^-)_2(TMPyP)]^{2+} + H_2O \rightarrow [Fe^{III}(NO)(TMPyP)]^{5+} + NO_2^- + 2OH^- \text{ (slow)} \quad (6b)$$

$$[Fe^{III}(NO)(TMPyP)]^{5+} \rightarrow [Fe^{III}(TMPyP)]^{5+} + NO \text{ (fast)} \quad (6c)$$

$$[Fe^{III}(NO)(TMPyP)]^{5+} \leftrightarrow [Fe^{II}(NO^+)(TMPyP)]^{5+} \text{ (fast)} \quad (6d)$$

$$[Fe^{II}(NO^+)(TMPyP)]^{5+} + NO \rightarrow [Fe^{II}(NO)TMPyP]^{4+} + NO^+ \text{ (fast)} \quad (6e)$$

$$NO^+ + H_2O \rightarrow NO_2^- + 2H^+ \text{ (fast)} \quad (6f)$$

Among these steps, the first step is the rate-determining step. Rigidly, this is not a first-order reaction because, besides $[Fe^{II}(NO_2^-)_2(TMPyP)]^{2+}$, H_2O or H^+ is also involved in the reaction. However, when using buffer, the concentration of H_2O or H^+ remains constant, and reaction 6b becomes a pseudo-first-order reaction. Since the overall disproportionation reaction (reaction 6a) is determined by the slowest step (reaction 6b), it also appears to be a pseudo-first-order reaction.

Electrochemical Generation of $[Fe^{II}(NO)(TMPyP)]^{4+}$. When reaction 5 is combined with reaction 6a, two new electrochemical reactions can be obtained:

$$[Fe^{II}(NO_2^-)_2(TMPyP)]^{2+} + H_2O + e^- \rightarrow [Fe^{II}(NO)(TMPyP)]^{4+} + NO_2^- + 2OH^- \quad (7)$$

$$[Fe^{III}(TMPyP)]^{5+} + NO_2^- + H_2O + 2e^- \rightarrow [Fe^{II}(NO)(TMPyP)]^{4+} + 2OH^- \quad (8)$$

Reaction 7 implies that $[Fe^{II}(NO_2^-)_2(TMPyP)]^{2+}$ can be further reduced to $[Fe^{II}(NO)(TMPyP)]^{4+}$ by one-electron transfer, and reaction 8 suggests $[Fe^{II}(NO)(TMPyP)]^{4+}$ can be electrochemically generated from a mixed solution of $[Fe^{III}(TMPyP)]^{5+}$ and NO_2^- at a low negative potential (-0.25 V).

Spectra were recorded during the electrochemical generation of $[Fe^{II}(NO)(TMPyP)]^{4+}$ at -0.25 V (see Figure 10). Two obvious electrolysis processes with different groups of isosbestic points were found to happen in sequence. The first process (with isosbestic points at 525 and 588 nm) corresponds to the rapid electrochemical formation of $[Fe^{II}(NO_2^-)_2(TMPyP)]^{2+}$, which has been discussed previously (see reaction 5). The second process (with isosbestic points at 544 and 576 nm) can be assigned to the further reduction of $[Fe^{II}(NO_2^-)_2(TMPyP)]^{2+}$ to $[Fe^{II}(NO)(TMPyP)]^{4+}$ (see reaction 7). It is obvious that the formation of $[Fe^{II}(NO_2^-)_2(TMPyP)]^{2+}$ is faster than that of $[Fe^{II}(NO)(TMPyP)]^{4+}$. This is because the formation rate of $[Fe^{II}(NO_2^-)_2(TMPyP)]^{2+}$ is determined by a relatively fast electrolysis process (reaction 5), whereas formation of $[Fe^{II}(NO)(TMPyP)]^{4+}$ is controlled by a relatively slow disproportionation process (see reactions 6a and 7). To confirm this, kinetic analysis was done on the electroreductive process of $[Fe^{II}(NO_2^-)_2(TMPyP)]^{2+}$ (reaction 7) shown in Figure 10, as it had been done for the disproportionation process of $[Fe^{II}(NO_2^-)_2(TMPyP)]^{2+}$ (reaction 6a). From the variation of spectral absorption at 550 nm with time, it was found that the reduction of $[Fe^{II}(NO_2^-)_2(TMPyP)]^{2+}$ to $[Fe^{II}(NO)(TMPyP)]^{4+}$ at -0.25 V (vs Ag/AgCl) is also a first-order reaction with a rate constant of $(7.85 \pm 0.44) \times 10^{-3}$ s^{-1} ($n = 7$, confidence level 95%). This value is very near that of the disproportionation reaction ($(7.30 \pm 0.36) \times 10^{-3}$ s^{-1}) described above, which implies that electrochemical reduction of $[Fe^{II}(NO_2^-)_2(TMPyP)]^{2+}$ to $[Fe^{II}(NO)(TMPyP)]^{4+}$ is controlled by disproportionation reaction rather than electrochemical reaction. Thus, the overall electrochemical reaction (reaction 7) maybe undergo reaction steps similar to those shown in reactions 6b−6f and an additional fast electrochemical reduction step similar to that shown in reaction 5. In addition to the spectroelectrochemical results described above, the difference in formation rate between $[Fe^{II}(NO_2^-)_2(TMPyP)]^{2+}$ and $[Fe^{II}(NO)(TMPyP)]^{4+}$ can be observed more clearly by cyclic voltammetry (see Figure 11). The scanning potential without preelectrolysis at -0.25 V gave rise to reversible redox peaks of $[Fe^{III}(TMPyP)]^{5+}/[Fe^{II}(NO_2^-)_2(TMPyP)]^{2+}$, indicating electrochemical formation of $[Fe^{II}(NO_2^-)_2(TMPyP)]^{2+}$ (reaction 5) is fast. In contrast, no redox peaks corresponding to $[Fe^{II}(NO)(TMPyP)]^{4+}$ in this case were observed. This means that the formation of $[Fe^{II}(NO)(TMPyP)]^{4+}$ is too slow at the time scale of cyclic voltammetry (several seconds), and thus, the amount of $[Fe^{II}(NO)(TMPyP)]^{4+}$ formed is too small to give a CV response. Until the preelectrolysis time was

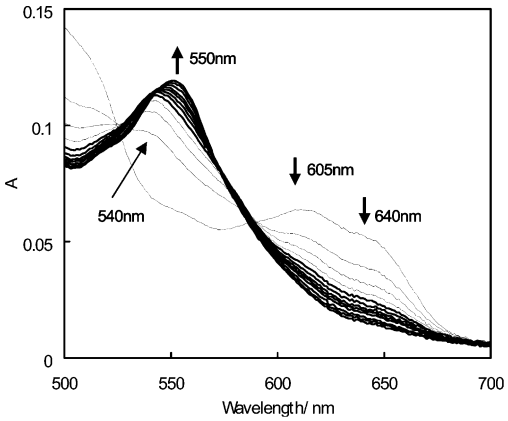

Figure 10. Electronic absorption spectral changes obtained during electrochemical generation of $[Fe^{II}(NO)(TMPyP)]^{4+}$ from the solution containing 2.5×10^{-4} mol·L^{-1} $[Fe^{III}(TMPyP)]^{5+}$ and 2.5×10^{-2} mol·L^{-1} $NaNO_2$ upon continuously applying -0.25 V. The spectra were recorded within 6 min.

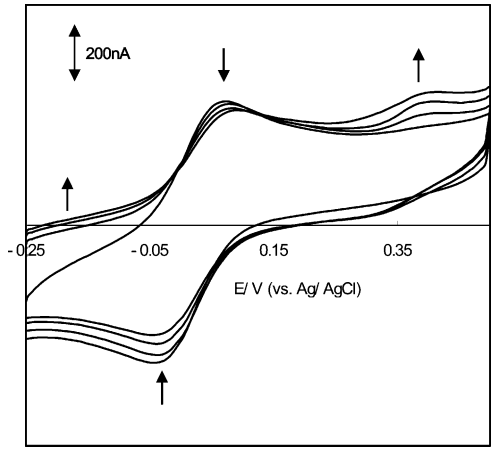

Figure 11. Cyclic voltammograms obtained for the solution containing 2.5×10^{-4} mol·L^{-1} $[Fe^{III}(TMPyP)]^{5+}$ and 2.5×10^{-2} mol·L^{-1} $NaNO_2$ at the Pt electrode after preelectrolysis at −0.25 V for 0, 2, 5, and 10 min. The scan rate was 10 mV·s^{-1}.

more than 2 min, the anodic wave corresponding to $[Fe^{II}(NO)(TMPyP)]^{4+}$ was observed to appear at 0.38 V,[38] suggesting that reduction of $[Fe^{II}(NO_2^-)_2(TMPyP)]^{2+}$ to $[Fe^{II}(NO)(TMPyP)]^{4+}$ was slow. According to Figure 10, whole cathodic electrolysis (reaction 8) can be completed within 6 min and eventually gave >95% conversion of $[Fe^{III}(TMPyP)]^{5+}$ to $[Fe^{II}(NO)(TMPyP)]^{4+}$.

The influence of applying a cathodic potential on the stability of $[Fe^{II}(NO)(TMPyP)]^{4+}$ was studied. It was found that $[Fe^{II}(NO)(TMPyP)]^{4+}$ was quite stable at the potential range from −0.20 to −0.35 V; however, it began to decompose when the potential was less than −0.40 V (vs Ag/AgCl), giving rise to $[Fe^{II}(TMPyP)]^{4+}$ as the final product. This indicates that coordinated NO can be further reduced to other nitrogen compounds such as nitrous oxide or ammonia when a high negative potential is applied.[34,35]

Release of NO from $[Fe^{II}(NO)(TMPyP)]^{4+}$. As shown in Figure 11, the anodic peak at +0.38 V has been confirmed to result from the oxidation of $[Fe^{II}(NO)(TMPyP)]^{4+}$,[35,38,46] the products of which were proposed to be $[Fe^{III}(TMPyP)]^{5+}$ and free NO.[46] To release NO from $[Fe^{II}(NO)(TMPyP)]^{4+}$, the oxidation potential should be chosen between +0.35 and +0.70 V, because when the potential is lower than +0.35 V, $[Fe^{II}(NO)(TMPyP)]^{4+}$ is difficult to oxidize (see Figure 11), and when the potential is higher than +0.70 V, $[Fe^{II}(NO)(TMPyP)]^{4+}$ will be oxidized to $[Fe^{III}(TMPyP)]^{5+}$ and NO_2^-.[38] In our study, the potential for oxidation of $[Fe^{II}(NO)(TMPyP)]^{4+}$ was chosen to be +0.40 V, under which a maximum oxidation rate of $[Fe^{II}(NO)(TMPyP)]^{4+}$ was obtained while undesirable side reactions were avoided. Figure 12 shows that, as soon as the +0.40 V potential is applied, the amount of $[Fe^{II}(NO)(TMPyP)]^{4+}$ (550 nm) decreases whereas the amount of $[Fe^{III}(TMPyP)]^{5+}$ (605 and 640 nm) increases with time, indicating that $[Fe^{II}(NO)(TMPyP)]^{4+}$ can be oxidized to $[Fe^{III}(TMPyP)]^{5+}$ at this potential. To confirm that NO rather than NO_2^- was another product during the oxidation of $[Fe^{II}(NO)(TMPyP)]^{4+}$ at the potential of +0.40 V, the potential was switched to −0.25 V, where $[Fe^{III}(TMPyP)]^{5+}$ could be reduced to $[Fe^{II}(TMPyP)]^{4+}$. If NO existed in the solution, it would combine

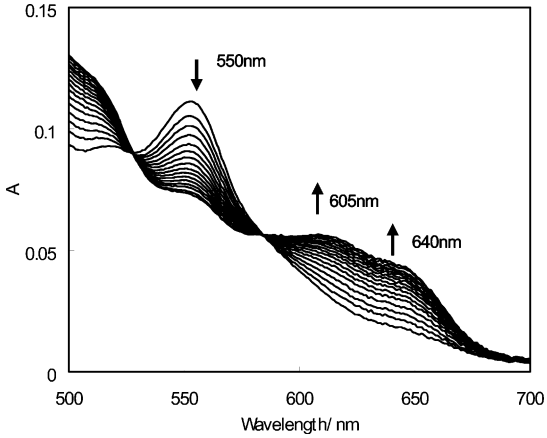

Figure 12. Electronic absorption spectral changes obtained for 2.5×10^{-4} mol·L^{-1} $[Fe^{II}(NO)(TMPyP)]^{4+}$ during anodic electrolysis at +0.40 V. The spectra were recorded within 2 min.

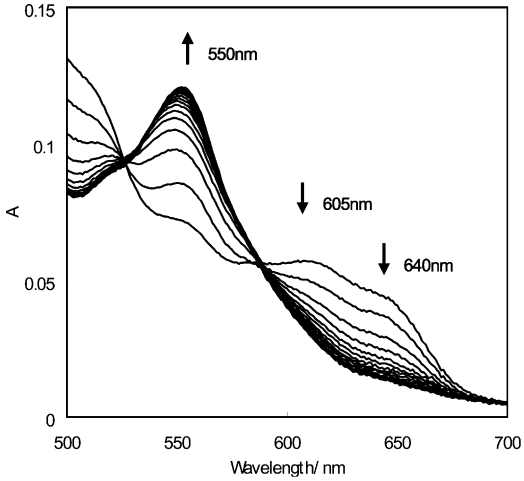

Figure 13. Electronic absorption spectral changes obtained for the final anodic product in Figure 12 during its re-reduction at −0.25 V. The spectra were recorded within 2 min.

with reproduced $[Fe^{II}(TMPyP)]^{4+}$ to form $[Fe^{II}(NO)(TMPyP)]^{4+}$, resulting in a gradual increase of the Q-band at 550 nm, while if NO_2^- was produced during oxidation at +0.40 V, when −0.25 V was applied, reaction 5 would happen, and an increase of the Q-band at 540 nm as shown in Figure 7 would be observed. Actually, Figure 13 shows that $[Fe^{II}(NO)(TMPyP)]^{4+}$ (550 nm) is restored after this redox cycle, which thus confirms that free NO is released into solution when $[Fe^{II}(NO)(TMPyP)]^{4+}$ is oxidized at +0.40 V:

$$[Fe^{II}(NO)(TMPyP)]^{4+} \rightarrow [Fe^{III}(TMPyP)]^{5+} + NO + e^- \quad (9)$$

Continuous Generation of Free NO. The electrochemical generation of free NO from nitrite requires the reduction at −0.25 V (see reaction 8) and the oxidation at +0.40 V (see reaction 9) in sequence. Thus, two electrolytic cells involved in a flow system (Figure 1) were utilized to realize continuous generation of free NO. Cell A was used for the generation of $[Fe^{II}(NO)(TMPyP)]^{4+}$. Cell B was used for the oxidation of $[Fe^{II}(NO)(TMPyP)]^{4+}$ to release free NO into the solution. By bubbling argon gas, NO was transferred from the solution phase to the gas phase in solution reservoir C, where the

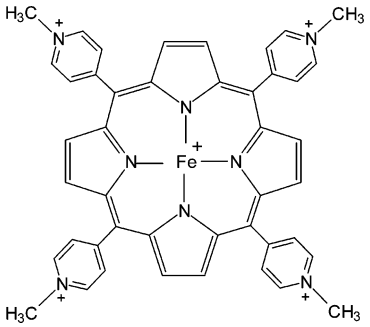

Figure 14. Chemical structure of $[Fe^{III}(TMPyP)]^{5+}$.

concentration of NO gas was monitored by the NO gas sensor. Because the cathodic electrolytic rate is controlled by the disproportionation of $[Fe^{II}(NO_2^-)_2(TMPyP)]^{2+}$, to ensure >90% conversion of $[Fe^{II}(NO_2^-)_2(TMPyP)]^{2+}$ to $[Fe^{II}(NO)(TMPyP)]^{4+}$, 5 min is essential for cathodic electrolysis. To meet the electrolytic time requirement, the electrolytic solution was pumped through the flow electrolytic cells (with a volume of 1.0 mL) at the rate of 200 μL/min. Under these conditions, a electrolytic solution containing 2.5×10^{-4} mol·L^{-1} $[Fe^{III}(TMPyP)]^{5+}$, 2.5×10^{-2} mol·L^{-1} $NaNO_2$, and 0.25 mol·L^{-1} PBS (pH 7.4) was used for flow electrolysis. Finally, a 75 ppm NO gas stream at a rate of 10 mL/min was obtained.

Discussion

Electrochemical generation of NO from NO_2^- can be catalyzed by $[Fe^{III}(TMPyP)]^{5+}$. First, at a low negative potential (−0.250 V vs Ag/AgCl), NO_2^- complexes with $[Fe^{II}(TMPyP)]^{4+}$ to yield an unstable intermediate, $[Fe^{II}(NO_2^-)_2(TMPyP)]^{2+}$, and then this complexes spontaneously but slowly changes to a stable coordinated NO, $[Fe^{II}(NO)(TMPyP)]^{4+}$, via a disproportionation reaction. At a low positive potential (+0.400 mV vs Ag/AgCl), free NO can be released into solution for the oxidation of $[Fe^{II}(NO)(TMPyP)]^{4+}$ to $[Fe^{III}(TMPyP)]^{5+}$ and NO. Thus, $[Fe^{III}(TMPyP)]^{5+}$ acts as a catalyst during the electrochemical generation of NO from NO_2^-.

Apparently, our experimental results showed that the interactions of nitrite and NO with ferrous and ferric porphyrins in aqueous solutions were quite different from those observed in nonaqueous media.

As described above, nitrite and NO did not complex with ferric porphyrin, $[Fe^{III}(TMPyP)]^{5+}$, at all in aqueous solution. In contrast, many other studies showed that either nitrite[28,33,39] or NO[32,48] could complex with ferric porphyrins to form five- or six-coordinate species in nonaqueous media. These unusual complexation behaviors of $[Fe^{III}(TMPyP)]^{5+}$ with nitrite and NO in aqueous solution are probably due to the unique chemical structure of $[Fe^{III}(TMPyP)]^{5+}$ and the effect of other strong axial ligands. As shown in Figure 14, $[Fe^{III}(TMPyP)]^{5+}$ carries five positive charges, which results in the central iron(III) being readily attacked by anionic ligands or even a water molecule. It is quite well-known that the crystal of $[Fe^{III}(TMPyP)]Cl_5$ is highly hygroscopic, which

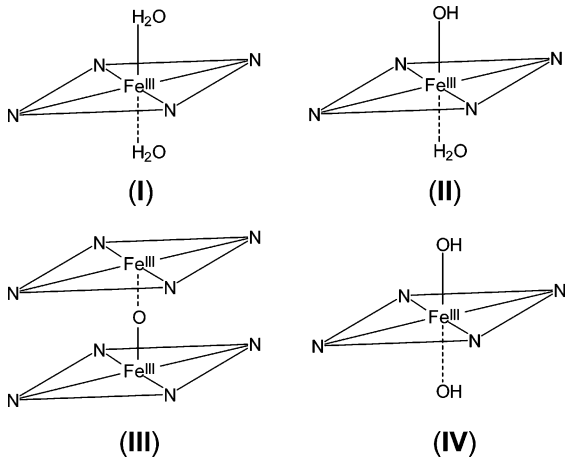

Figure 15. Various $[Fe^{III}(TMPyP)]^{5+}$ species in aqueous solution.

means that the porphyrin is readily combined with H_2O. And it was reported that, in aqueous solution, $[Fe^{III}(TMPyP)]^{5+}$ interacted with H_2O and OH^- to form various five- or six-coordinate species (see Figure 15, I−IX),[42,49] depending on the solution pH and the concentration of $[Fe^{III}(TMPyP)]^{5+}$. At a low pH value (pH < 6), most $[Fe^{III}(TMPyP)]^{5+}$ existed in a diaquo six-coordinated complex (species I), at a high pH value (pH > 11), $[Fe^{III}(TMPyP)]^{5+}$ was mainly present in the form of a dihydroxy complex (species IX),[49] and at a medium pH value, there was a concentration-determined dimer equilibrium between a monohydroxy complex (species II) and a μ-oxo dimer (species III). The monohydroxy complex was proved to exist in diluted solution, whereas the μ-oxo dimer was present in concentrated solution or in the crystal.[42] Probably, it was just this kind of strong electrostatic interaction of $[Fe^{III}(TMPyP)]^{5+}$ with other stronger ligands, especially OH^- in aqueous solution, that competitively blocked the complexation of $[Fe^{III}(TMPyP)]^{5+}$ with nitrite and NO. In contrast, in nonaqueous media, the complexation of ferric porphyrins with nitrite or NO was often observed. This was probably due to the different complexation conditions in nonaqueous solution. Generally, the strong axial ligand OH^- was absent in nonaqueous media, so ferric porphyrins could complex with nitrite via electrostatic interaction without being competitively blocked by this strong ligand. The effect of other strong axial ligands on the complexation of ferric porphyrins with nitrite has been confirmed by Fernandes and co-workers.[33] It was reported that, in nonaqueous solution, if a stronger axial ligand, Cl^-, was present, nitrite did not complex with ferric porphyrin. Only when the concentration of nitrite was high enough to displace chloride could the complex reaction happen, giving rise to bisnitrite complexes of ferric porphyrin. It is evident that strong ligands tend to prevent the complex reaction of ferric porphyrins with nitrite and NO.

Unlike $[Fe^{III}(TMPyP)]^{5+}$, $[Fe^{II}(TMPyP)]^{4+}$ was found to readily complex with both nitrite and NO in aqueous solution. These different behaviors can be explained by the difference in electronic structures of ferric and ferrous porphyrins. When

(48) Settin, M. F.; Fanning, J. C. *Inorg. Chem.* **1988**, *27*, 1431−1435.

(49) Bell, S. E. J.; Hester, R. E.; Hill, J. N.; Shawcross, D. R.; Linsay Smith, J. R. *J. Chem. Soc., Faraday Trans.* **1990**, *86*, 4017−4023.

Scheme 1

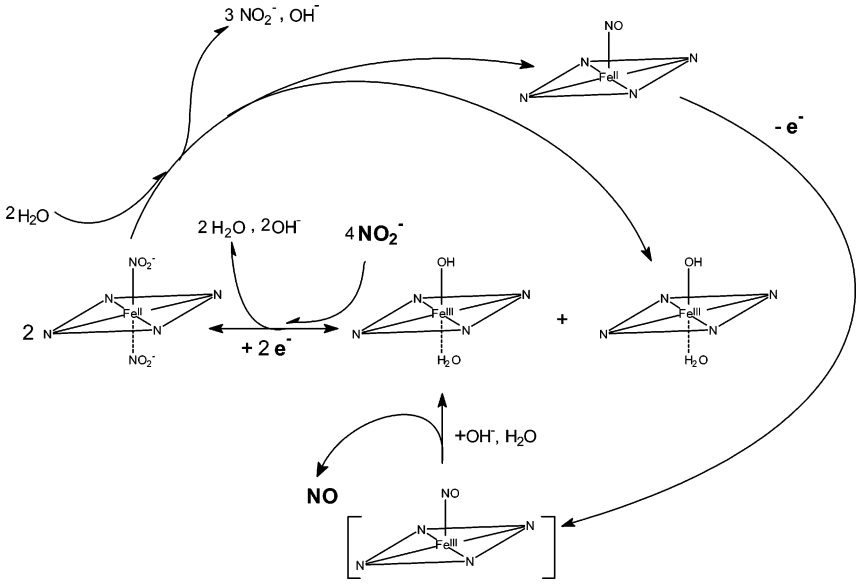

$[Fe^{III}(TMPyP)]^{5+}$ is reduced to $[Fe^{II}(TMPyP)]^{4+}$, the electron density of the central iron increases, resulting in a decrease of the electrostatic interaction between the iron(II) center and anionic ligands, such as Cl^-, OH^-, and NO_2^-. However, ferrous porphyrin (d^6) has one additional d-orbital electron compared to ferric porphyrin (d^5), which gives ferrous porphyrins a much stronger orbital interaction ($d_\pi \rightarrow \pi^*$) with strong π-accepting ligands, such as nitrite[50] and NO.[51] In fact, besides $[Fe^{II}(TMPyP)]^{4+}$, many other ferrous porphyrins can complex with nitrite or NO.[31,32,47,50]

Although both nitrite and NO can complex with $[Fe^{II}(TMPyP)]^{4+}$, the thermodynamic stabilities of nitrite- and NO-coordinated ferrous porphyrins are quite different; the latter is much more stable than the former. This difference was confirmed by our experiments. First, the half-wave potential of oxidation of $[Fe^{II}(NO)(TMPyP)]^{4+}$ was more positive than that of $[Fe^{II}(NO_2^-)_2(TMPyP)]^{3+}$ (see Figure 11), which means that NO complexes with $[Fe^{II}(TMPyP)]^{4+}$ more strongly than nitrite does, and thus makes the oxidation of ferrous iron to ferric iron more difficult. Second, it was clearly evident that $[Fe^{II}(NO_2^-)_2(TMPyP)]^{3+}$ spontaneously changed into $[Fe^{II}(NO)(TMPyP)]^{4+}$ and $[Fe^{III}(TMPyP)]^{5+}$ via disproportionation (see Figures 4, 8, and 10). This spontaneous reaction appears to result from the extreme thermodynamic stability of the nitrosyl−ferrous porphyrins, $[Fe^{II}(NO)(TMPyP)]^{4+}$. For the same reason, disproportionation reactions were observed for other coordinated iron porphyrin systems, such as iron(III)−nitrite,[28,39] iron(III)−NO,[48] and iron(II)−nitrite.[52] These disproportionation reactions commonly yielded a stable iron(II)−nitrosyl species, although different reaction pathways were undergone; for example, for ferrous porphyrins, electrons were transferred from iron(II) to nitrite whereas, for ferric porphyrins, electrons were donated to iron(III) by ligands (nitrite or NO).

Just because of the extreme stability of $[Fe^{II}(NO)(TMPyP)]^{4+}$, it was impossible to decompose this complex into NO and $[Fe^{II}(TMPyP)]^{4+}$ by bubbling argon gas; i.e., it was impossible to shift the complex equilibrium to the left in eq 2. It means that we cannot obtain free NO by bubbling argon gas into $[Fe^{II}(NO)(TMPyP)]^{4+}$ solution. Fortunately, according to our experimental results (see Figures 12 and 13), we found that $[Fe^{II}(NO)(TMPyP)]^{4+}$ could be oxidized into $[Fe^{III}(TMPyP)]^{5+}$ and free NO at a low positive potential (ca. +400 mV vs Ag/AgCl). It was evident that oxidation of $[Fe^{II}(NO)(TMPyP)]^{4+}$ was an irreversible process, because only an anodic peak for the oxidation of $[Fe^{II}(NO)(TMPyP)]^{4+}$ was found at +0.38 V (see Figure 11); no corresponding cathodic peak was observed. This implies that $[Fe^{III}(NO)(TMPyP)]^{5+}$ does not exist stably in the aqueous solution. Maybe $[Fe^{III}(NO)(TMPyP)]^{5+}$ was produced, but attacked by some strong anodic ligands, mostly OH^-, and decomposed into $[Fe^{III}(TMPyP)]^{5+}$ (the actual molecular structure is much more complex as shown in Figure 15) and free NO rapidly. Thus, from our viewpoint, the effect of ligands is also very important for the decomposition of nitrosyl−ferric porphyrins just as it is important for the formation of nitrite or nitrosyl−ferric porphyrins (already discussed above). The effect of ligands or the displacement of NO ligand bound to the iron(III) center of porphyrins by other strong axial ligands can also be found in other nitrosyl−ferric porphyrin systems, such as $Fe^{III}(NO)(OEP)$, $Fe^{III}(NO)(OEC)$, and $Fe^{III}(NO)(OEiBC)$, in nonaqueous media.[32] When a sufficient amount of *N*-methylimidazole was added to these nitrosyl−ferric porphyrin solutions, NO was displaced and released into solution. This is analogous to our discovery that NO in $[Fe^{III}(NO)(TMPyP)]^{5+}$ was displaced by OH^- and released into aqueous solution.

In summary, our studies found that $[Fe^{III}(TMPyP)]^{5+}$ did not complex with nitrite or NO, probably for its strong

(50) Nasri, H.; Ellison, M. K.; Krebs, G.; Huynh, B. H.; Scheidt, W. R. *J. Am. Chem. Soc.* **2000**, *122*, 10795−10804.
(51) McCleverty, J. A. *Chem. Rev.* **2004**, *104*, 403−418.
(52) Lancaster, J. R.; Vega, M. J.; Kamin, H.; Orme-Johnson, N. R.; Orme-Johson, W. H.; Krueger, R. J.; Siegel, L. M. *J. Biol. Chem.* **1979**, *254*, 1268.

electrostatic interaction with OH^- in the aqueous solution, whereas $[Fe^{II}(TMPyP)]^{4+}$ could complex with both nitrite and NO maybe via a strong orbital interaction ($d_\pi \rightarrow \pi^*$), giving rise to $[Fe^{II}(NO_2^-)_2(TMPyP)]^{2+}$ and $[Fe^{II}(NO)(TMPyP)]^{4+}$, respectively. $[Fe^{II}(NO_2^-)_2(TMPyP)]^{2+}$ was not stable, and could be reduced to a much more stable species, $[Fe^{II}(NO)(TMPyP)]^{4+}$, by a pseudo-first-order disproportionation reaction. At low potential (ca. +400 mV vs Ag/AgCl), $[Fe^{II}(NO)(TMPyP)]^{4+}$ was irreversibly oxidized, yielding $[Fe^{III}(TMPyP)]^{5+}$ and releasing free NO into solution. The irreversible oxidation possibly involved formation and rapid decomposition of $[Fe^{III}(NO)(TMPyP)]^{5+}$ intermediate in the presence of a strong axial ligand, OH^-, in the aqueous solution. The overall mechanism for electrochemical generation of NO from nitrite catalyzed by $[Fe^{III}(TMPyP)]^{5+}$ in aqueous solution is proposed in Scheme 1. On this basis, a method for electrochemical generation of free NO with a high yield has been developed.

IC049323C